Reaction Kinetics, Mechanisms and Catalysis (2025) 138:1453–1467
https://doi.org/10.1007/s11144-025-02808-0

Esterification of free fat acids from waste cooking oil using $BiVO_4$ photocatalysts under visible irradiation

Camilo Aurélio Brandão Crisóstomo · Fernanda Barbosa Damaceno · João Paulo de Mesquita · Juliana Arriel Torres · Caue Ribeiro · Roberto Ananias Ribeiro, et al. ***[full author details at the end of the article]***

Received: 3 December 2024 / Accepted: 8 February 2025 / Published online: 19 February 2025

Abstract

Herein, we report the FFA photoesterification of waste cooking oil (WCO) using a $BiVO_4$ and visible irradiation. Despite undergoing treatments under different temperatures (120 °C and 150 °C), both synthesized samples presented high crystallinity and similar morphologies, corresponding to a mixture composed of the scheelite structure of monoclinic and tetragonal phases of $BiVO_4$. The FFA conversions with the photocatalysts were significantly higher than the non-catalytic reactions. The gas chromatography analysis shows that the products are composed of a mixture of ethyl esters and a low amount of fatty acid ethyl esters (FAEE). The results demonstrate that the photoesterification of FFA of non-edible vegetable oils can be driven by $BiVO_4$ photocatalysts under visible irradiation, at regular temperature, reduced ethanol/oil molar ratio, and short times.

Graphical Abstract

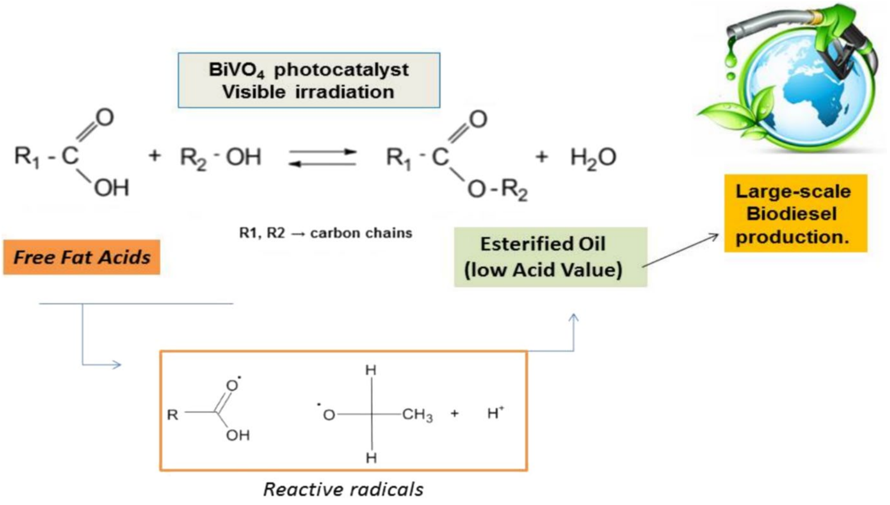

Keywords Bismuth vanadate · Waste cooking oil · Free-fat acids · Photoesterification · Ethyl esters · Fatty acid ethyl esters

Introduction

The bismuth vanadate ($BiVO_4$) is considered a *n-type* semiconductor with great attention for different applications due to its unique properties [1–9]. $BiVO_4$ is a non-toxic material chemically stable in aqueous media, and it can be applied where corrosion is not a concern. Other interesting properties include ferroelasticity, ionic conductivity, electrochemical properties, good dispersibility, corrosion resistance, and visible light absorption [2–4, 7–11].

The $BiVO_4$ presents a band gap (Eg) of about 2.4 eV and good mobility of the photogenerated charges [12, 13]. In this way, the $BiVO_4$ can be photoexcited by visible radiation beyond ultraviolet radiation, allowing, for instance, a broad absorption of solar radiation [14, 15].

Therefore, $BiVO_4$ is studied for many applications, such as photocatalysis [7, 8, 16], water splitting [8, 17, 18], and photodegradation of organic compounds, such as dyes [19, 20], pesticides [21], antibiotics [22, 23] and others [8, 24, 25]. Although knowledge about the role of semiconductors in photo-oxidative processes is already well established, there is a lack of studies about their utilization for biodiesel production compared to other applications [26–30]. Most studies demonstrate the application of semiconductors to different areas, such as hydrogen generation [31, 32].

Biodiesel production from oils (vegetable and animal oils, including waste cooking oils—WCO) consists of a two-step catalytic process, where free fatty acids (FFA) in the oil are initially esterified in the presence of an alcohol (methanol or ethanol), reducing the FFA concentration, followed by the transesterification of triglycerides with alcohol, which is catalyzed by NaOH (second step). The first step is critical since significant amounts of FFA in highly acidic oils can cause soap formation, reducing the yield of biodiesel production [26, 28–30]. Photoesterification can reduce the complexity of the whole process due to its simplicity, and a variety of semiconductors, including ZnO/SiO_2, Cr/SiO_2, TiO_2, $La^{3+/}ZnO\text{-}TiO_2$, $TiO_2/g\text{-}C_3N_4$, CdS, and WO_3, have been used as photocatalysts in the biodiesel production from different oils [33–35].

In addition to the importance of reducing the FFA of the oils, photocatalyst preparation may also be considered a concrete bottleneck to large-scale biodiesel production. The synthesis must be simple, low-cost, save energy, and allow the control of the particle properties. Some studies report the synthesis of $BiVO_4$ at different methods and temperatures [5, 36]. Among the different methods, the hydrothermal method is one of the most used, mainly due to its low temperatures (primarily heated up to 200 °C) and short synthesis times. Furthermore, the hydrothermal method can easily adjust the crystal structure and morphology [5, 9, 13, 36, 37].

Herein, we report the hydrothermal synthesis of $BiVO_4$ photocatalysts by the hydrothermal method under soft conditions. The $BiVO_4$ presented photoactivity for the FFA esterification of waste cooking oil (WCO) under visible irradiation, which is very promising for use before the transesterification process for biodiesel production.

Experimental

Materials preparation and characterization

Bismuth vanadate ($BiVO_4$) was synthesized using the oxidant peroxide method (OPM), followed by hydrothermal treatment [5]. Typically, 0.69 g of Bi $(NO_3)_3.5H_2O$ (bismuth subnitrate, 99.0%—Vetec Sigma) and 0.16 g of NH_4VO_3 (ammonium metavanadate, 99.0%—Vetec Sigma) were added to distilled water (40 mL) under stirring at room temperature. The Bi: V molar ratio used for the synthesis was 1:1. After 30 min, hydrogen peroxide (40% H_2O_2) was added to the mixture using a H_2O_2:Bi molar ratio of 10:1. Then, 40 mL of distilled water was added to the suspension, and the formed complex was placed into a Teflon vessel heated in a stainless-steel autoclave at 120 °C or 150 °C for 5 h of hydrothermal treatment. These prepared samples were referred to as $BiVO_4$-120 and $BiVO_4$-150, respectively. Finally, the prepared catalysts were washed firstly with distilled water and, secondly, with isopropyl alcohol. After that, the catalysts were centrifuged and dried at 70 °C for 2 h.

The X-ray (powder) diffraction (XRD) analysis was obtained in a Shimadzu XRD-6000 diffractometer with monochromatic Cu K_α radiation ($\lambda = 0.15406$ nm) using a scanning rate of 2°/min with 2θ ranging from 10 to 70°. Fourier transform infrared spectra (FTIR) were obtained using a Varian 640-IR FTIR Spectrometer from 400 to 4000 cm^{-1}. The morphology was examined by Scanning electron microscopy (SEM), using a Hitachi TM-3000 microscope, and the elemental composition was evaluated by Energy dispersive spectroscopy (EDS) with the detector Oxford Swift ED 3000. The average values of the elemental compositions were calculated by the mean of the values registered in three different regions of the samples. Diffuse reflectance spectrometry (DRS) data were obtained in a UV–vis spectrophotometer—Shimadzu UV-2600, and the band gap values were calculated using the Tauc equation [38]. Zeta potential analyses were carried out on a Malvern® Zetasizer Nano instrument. For the analysis, 1 mg of material was dispersed into 10 mL of deionized water and taken for sonication. Aqueous solutions of hydrochloric acid (HCl, Synth®) and sodium hydroxide (NaOH, Synth®) were added to adjust the pH during each analysis step.

Photoesterification tests

The photoesterification tests were carried out using a photoreactor equipped with six (6) fluorescent lamps emitting visible radiation. The waste cooking oil (WCO) was obtained from a restaurant. The WCO was filtered before the tests. Absolute ethanol was of analytical grade (> 99%, Synth). The tests were performed at 40 °C under visible lamps placed on the top of the photoreactor (15 W power and distance of 0.24 m from the reaction mixture). It was used the following conditions: photocatalyst concentration of 1 wt% in relation to the initial WCO mass; ethanol: WCO molar ratio of 5:1; and stirring speed of 400 rpm. These reaction conditions were based on previous studies [27, 29]. A blank experiment (without the catalyst) was also tested under the same conditions. After the reactions, the mixture was placed in a separation funnel until the two liquid phases separated. The oil layer (upper part) was centrifuged to remove the catalyst, and the supernatant was used for subsequent determination of the Acid Value (AV). The AV of the initial WCO and reaction products were determined following the AOCS Cd-3d-63 method of the American Oil Chemists Society (AOCS) by titrating the sample with NaOH at 0.1 mol L^{-1}.

The AV (mg KOH g^{-1}) was determined using the Eq. 1 [26, 28]:

$$AV = \frac{V \times f \times C \times 56.11}{m} \tag{1}$$

Here V is the volume of the standard solution of NaOH (in mL) that was consumed until it reaches the titration endpoint; f is the NaOH solution correction factor; C is the concentration of NaOH standard solution (mol/L); 56.11 is the molar mass of KOH ing/mol); m is the weight (g) of the test sample. Also, the FFA conversion (% C_{FFA}) during the esterification was determined using Eq. 2:

$$\%C_{FFA} = \frac{AV_i - AV_f}{AV_i} \times 100 \tag{2}$$

The products compositions were determined by gas chromatography using a flame ionization detector (FID), according to the adapted EN-14103 method. The description is contained in the supplementary material.

Results and discussion

Characterization of the $BiVO_4$ samples

Fig. 1 shows the XRD patterns obtained for the synthesized catalysts compared with the standard pattern of the monoclinic scheelite phase (JCPDS no. 75–1866 and ICSD 62706). Both synthesized $BiVO_4$ materials showed similar diffractograms, with the main peaks corresponding to the monoclinic scheelite crystalline phase of $BiVO_4$, at 2θ equal to 18.8, 29.1, 30.9 (highest), 35.1, 40.4, 42.8, 46.0, 47.7, 50.4, 53.7, 56.1, 58.2° and 59.2°, which are indexed to the crystallographic planes (101), (112), (004), (020), (211), (015), (240), (042), (202), (161), (204), (321) and (123) [9, 39–41].

However, other diffraction peaks were observed in the synthesized samples, such as the peaks at 2θ at around 24.1° and 33.4°, indexed to the crystallographic planes (200) and (112) of the tetragonal scheelite $BiVO_4$ phase [JCPDS no. 14–0133]. There are other peaks in these diffractograms. The peaks at 2θ next to 12° and 26° were not completely identified, probably ascribed to secondary phases of Bi [42].

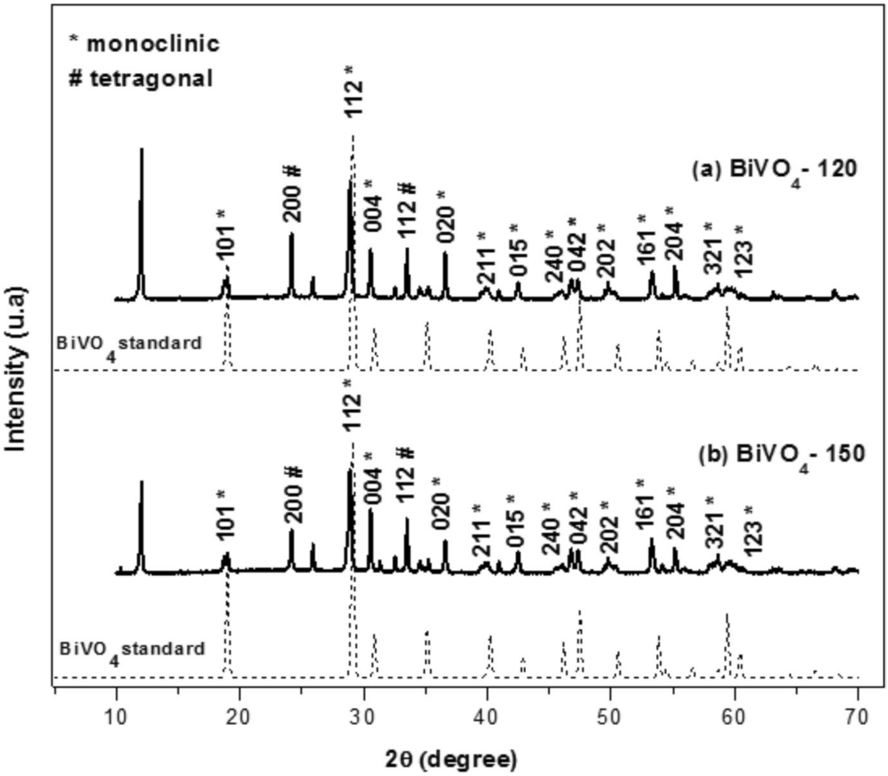

Fig. 1 XRD patterns obtained for the $BiVO_4$ samples. (---) standard XRD patterns of the monoclinic crystalline phases of the $BiVO_4$

Thus, the hydrothermal treatment apparently led to the formation of a mixture of crystalline phases, which are mainly composed of scheelite structures from monoclinic and tetragonal phases of $BiVO_4$. It is worth pointing out that the monoclinic phase of $BiVO_4$ is considered the most photoactive in photocatalytic processes. However, some authors demonstrated the monoclinic/tetragonal heterojunction could also improve the charge (electron/hole) separation, reducing the charge recombination [6, 14, 15]. Also, it was possible to observe that the variation in temperature during the synthesis did not cause significant changes in the structure of the studied materials, and has only resulted in peaks with different intensities. The results are in accordance with other studies that have also used the hydrothermal method for the synthesis of $BiVO_4$ and obtained a mixture of scheelite phases [3, 9, 13, 36, 39–41, 43].

The FTIR spectra of the samples are shown in Fig. 2, and the main vibration modes are in Table 1. The FTIR spectra are typical of the $BiVO_4$ [3, 9, 13, 16, 36, 39, 44, 45].

The similarity between the two spectra demonstrates that the increase in synthesis temperature did not significantly influence the functional groups on the

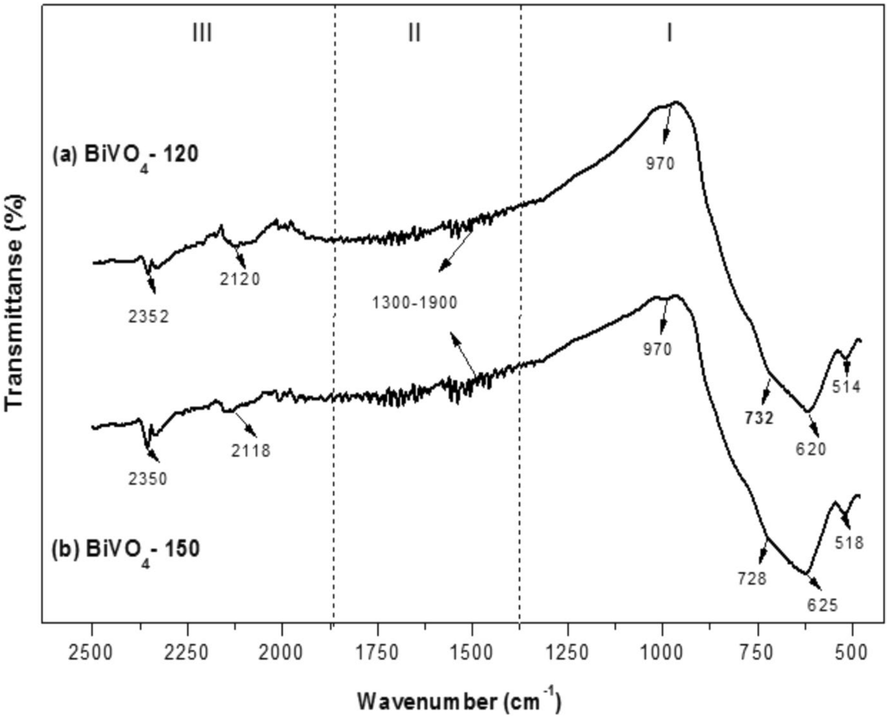

Fig. 2 FTIR spectra of the synthesized $BiVO_4$ samples

Table 1 Vibration modes of the synthesized $BiVO_4$ samples

Wavenumber (cm^{-1})	Vibration mode
2120 and 2360	H–O–H bond Angular deformation
1300–1900	H–O–H bond Angular deformation
970	V=O stretching of vanadyl
615	Deformation of the V–O bond; Vibration of the Bi–O bond
510	Stretching of the V–O bond and Bi–O–V bond
470	VO_4^{3-} symmetric angular deformation

studied material's surface. In region I, the bands between 470 and 840 cm^{-1} are typical of vibration modes present in the monoclinic $BiVO_4$ in accordance with the XRD results [3, 13, 16, 36, 39, 45]. The band at 470 cm^{-1} is attributed to VO_4^{3-} symmetric angular deformation [36]. Bands next to 510 cm^{-1} are related to the stretching of the V–O and Bi–O–V bonds, whereas the bands next to 615 cm^{-1} are related to the deformation of the V–O bond and the vibration of the Bi–O bond. Bands at about 970 cm^{-1} are characteristics of V = O stretching [46]. The small bands in region II (1300 to 1900 cm^{-1}) are ascribed to water and organic impurities [3, 9, 16, 36]. Also, the bands in region III (2120 and 2360 cm^{-1}) are associated with the angular deformation of H–O–H bond.

Fig. 3 shows the representative images obtained by scanning electron microscopy (SEM). The images demonstrate that the synthesized samples comprise two different morphologies, possibly related to the two phases identified in XRD, formed by micrometric aggregates. It is worth pointing out that the morphology observed is significantly different from the literature [5]; it indicates the change in the reaction time changed the growth process, and the short reaction time resulted in the formation of samples with smaller particle sizes. The elemental compositions of both samples were also obtained by EDS (Table 2). As can be seen, the samples showed a slight difference between the compositions of Bi and V, being that the Bi/V molar ratio of the sample $BiVO_4$-150 was similar to the theoretical value for $BiVO_4$, i.e., 1:1 (Bi:V equal to 1.3).

Fig. 4a presents the UV–visible (DRS) spectra of the obtained $BiVO_4$ materials, and the values of band gap energy (*Eg*) were determined by using the Tauc plot for a direct transition semiconductor [38], as shown in Fig. 4b. The absorption edges

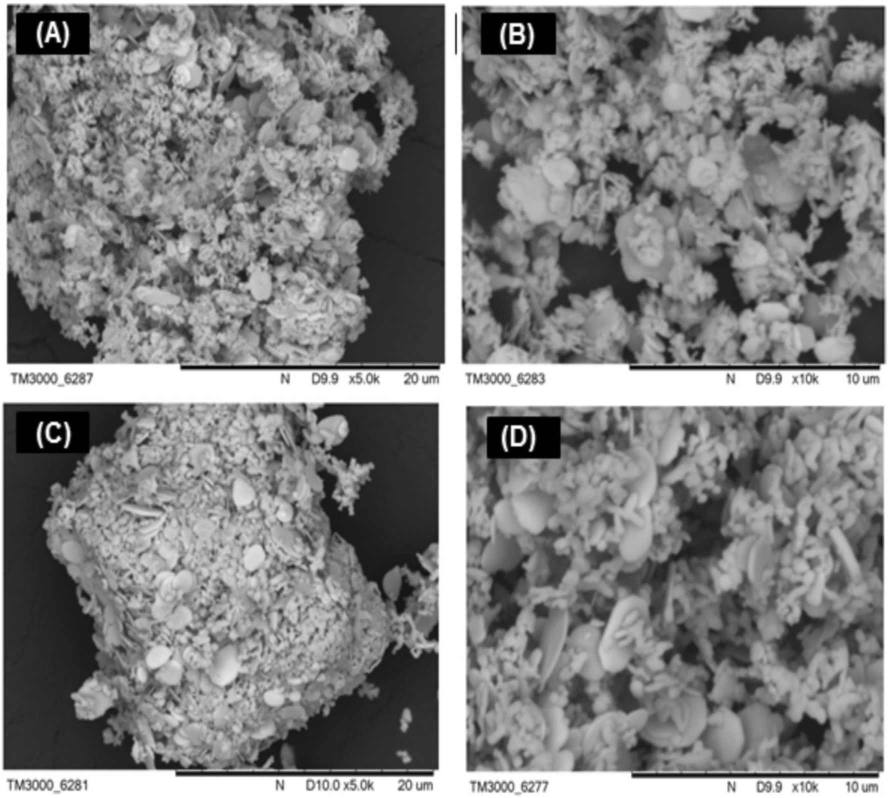

Fig. 3 Representative SEM images of the synthesized $BiVO_4$ samples. $BiVO_4$-120: A, and B; $BiVO_4$-150: C and D

Table 2 Elemental composition (% mol) of the synthesized samples and Bi/V molar ratios obtained by EDS

Element	$BiVO_4$-120	$BiVO_4$-150
Oxygen	62%	61%
Vanadium	13%	17%
Bismuth	25%	22%
Bi/V	1.9	1.3

of both $BiVO_4$ samples were at approximately 470 nm, suggesting that the synthesized samples are visible light-responsive photocatalysts, i.e., the electron transition occurs in the visible region. The corresponding band gap values (~ 2.4 eV) were very similar, and they are in accordance with reported values [3, 41, 46]. This *Eg* value indicated that the $BiVO_4$ is photoactivated under visible irradiation.

Fig. S1 shows the zeta potential for the samples of $BiVO_4$ as a function of pH. These results demonstrate that both synthesized samples present a similar and low isoelectric point (IEP equal to 2.1 and 1.9 for samples $BiVO_4$-120 and $BiVO_4$-150, respectively), and both samples are probably stable under pH higher than 4.

FFA photoesterification over $BiVO_4$

First, the fatty acid profiles (bonded to the glycerol in the triglyceride molecule) in the WCO were analyzed using gas chromatography equipped with a flame ionization detector. Also, the FFA total content (%) was determined by the AOCS Cd-3d-63 method by titrating the sample (described in the experimental section). The results are shown in Table S1, and the WCO presented an Acid Value (AV) equal to 15.8 mg KOH g^{-1}, corresponding to 7.9% of the total content of FFA.

In the sequence, tests without (and with) the catalysts were carried out without radiation or by using visible irradiation. These tests were carried out with molar ratios equal to 20:1 or 5:1 (ethanol:oil). Tables 3 and 4 summarize all these results.

The photoesterification tests were firstly conducted at ethanol: oil molar ratios of 20:1 at a fixed temperature equal to 40 °C (Table 3). In the non-catalytic test (without the synthesized $BiVO_4$ samples), the FFA conversion (C_{FFA}) was around 45%. In this molar ratio, no significant increase in the FFA conversion (around 1.1%) was observed using both synthetized $BiVO_4$ samples compared to the non-catalytic test. Also, in the photoesterification non-catalytic test, the visible irradiation had no significant effect, since the FFA conversion was most probably due to the high ethanol:oil molar ratio (20:1).

On the other hand, in the non-catalytic tests using a molar ratio equal to 5:1 (ethanol:oil), the FFA conversion dropped significantly to lower values ($< 10\%$). Also, the FFA conversion observed with the $BiVO_4$ photocatalysts using a 5:1 molar ratio was greater than the non-catalytic test (approximately 6 times for sample $BiVO_4$-120 under visible irradiation). Thus, these results indicate that the reaction of esterification using the highest ethanol: oil molar ratio (20:1) occurs due to excess of alcohol and not because of the photocatalyst. In this way, the photoactivity of $BiVO_4$ samples could be evidenced by reducing the ethanol: oil molar ratio to 5:1.

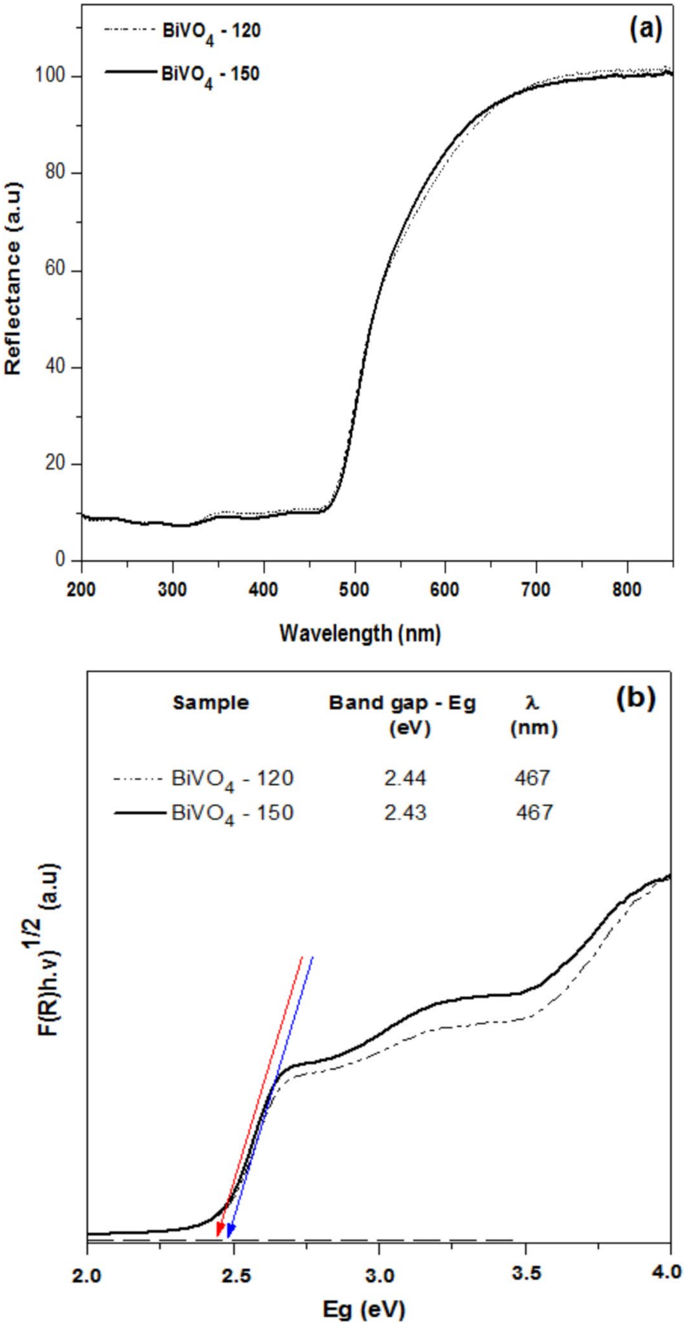

Fig. 4 **a** Spectra obtained by UV–vis diffuse reflectance (DRS) for the both $BiVO_4$ samples; **b** Tauc plot for the direct allowed transition obtained from DRS data (band gap values (Eg) are also shown in the inset

Table 3 FFA conversion (C_{FFA}) obtained by using an ethanol:oil molar ratio of 20:1

Sample	Irradiation	AV final (mg KOH/g)	FFA final (%)	FFA conversion (%)	Increase in FFA conversion*
Non-catalytic	–	8.9	4.4	43.6	–
	Visible	8.7	4.3	44.9	–
$BiVO_4$-120	–	8.2	4.1	47.5	1.1 x
	Visible	8.3	4.1	47.4	1.1 x
$BiVO_4$-150	–	8.5	4.2	46.0	1.1 x
	Visible	8.5	4.2	46.2	1.1 x

*In relation to non-catalytic test without irradiation (blank)

Table 4 FFA conversion (C_{FFA}) obtained by using an ethanol:oil molar ratio of 5:1

Sample	Irradiation	AV final (mg KOH/g)	FFA final (%)	FFA conversion (%)	Increase in FFA conversion*
Non-catalytic	–	15.1	7.6	4.1	–
	Visible	14.7	7.3	6.8	–
$BiVO_4$-120	–	13.4	6.7	15.2	3.7 x
	Visible	8.9	4.5	43.1	10.5 x
$BiVO_4$-150	–	13.2	6.6	16.1	3.9 x
	Visible	9.2	4.6	41.4	10.1 x

* In relation to non-catalytic test without irradiation (blank)

Furthermore, it is possible to observe (Tables 3 and 4) that the temperatures of hydrothermal synthesis slightly affect the FFA. The highest FFA conversion was obtained using $BiVO_4$-120 under visible irradiation, obtaining the esterified oil with approximately 4.5% FFA content. The use of low temperatures of synthesis and visible radiation are both interesting from the environmental and sustainable point of view.

Table S2 shows the comparison between our results for photoesterification and literature data. Remarkably, our results used more moderate reaction conditions than reported in other studies, especially shorter times and visible irradiation (instead of UVC).

A basic mechanism of the photoesterification reaction is described in the literature by following the sequence of three steps [27, 29, 47, 48]. Fig. S2 shows a proposed reaction scheme for the photo esterification of FFA with ethanol. Initially, there is the adsorption of the ethanol (CH_3–CH_2–OH) and the FFA's (HOOC–R) on the photocatalysts surface, mainly due to the presence of active acid sites that may act as Lewis sites. In the sequence, the formation of holes (h^+) and electrons (e^-) promotes: (a) the reduction reaction of the HOOC–R with (e^-) produces the •OHOC-R radicals; (b) and, at the same time, the (h^+) reacts with

Table 5 Ethyl esters qualitative profile in the obtained product (esterified oil) using $BiVO_4$-120 and the ethanol:oil molar ratio of 5:1

Compound	Carbons	Content (wt %) after photoesterification	
		–	Visible
Ethyl palmitate	C16:0	9.9	11.8
Ethyl stearate	C18:0	5.5	5.7
Ethyl oleate	C18:1	37.2	31.8
Ethyl linoleate	C18:2	41.6	44.5
Ethyl α-linolenate	C18:3	6.0	6.3

the CH_3–CH_2–OH, producing CH_3–CH_2–O• radicals and ions (H^+). Both reactions occur through the absorption of photons on the photocatalyst surface. (c) After that, the ions (H^+) and radicals formed (CH_3–CH_2–O• and •OHOC–R) can react to form ethyl ester and water. Finally, the products are desorbed and migrate to the liquid phase.

Table 5 shows the qualitative profile of the final product obtained in the photocatalytic tests under visible irradiation (and in the absence of light) using an ethanol: oil molar ratio of 5:1. Thus, it was verified that the obtained product (esterified oil with a low acidity) is composed of a mixture of ethyl esters formed by the photoesterification of free fat acids and, probably, other amounts of fat acid ethyl esters (FAEE) formed by the conversion of the triglycerides by direct photo transesterification. The presence of degradation sub-products was not observed, in the oil phase of the products.

Lastly, the process presented here can be activated by solar irradiation and avoids some drastic conditions frequently used in the FFA esterification. Also, the use of $BiVO_4$ as catalyst and WCO as a raw material can reduce the cost for the production of biodiesel.

Conclusion

We have demonstrated the performance of $BiVO_4$ for the esterification and photoesterification of FFA present in WCO. The synthesis by hydrothermal treatment led to the formation of a mixture of crystalline phases of $BiVO_4$. The temperature of the hydrothermal synthesis did not significantly affect the morphologies, structures, and chemical groups on the studied material's surface. The activity of $BiVO_4$ samples for the photoesterification of FFA from WCO was only evidenced using the ethanol: oil molar ratio of 5:1. The highest FFA conversion was obtained using the $BiVO_4$-120 photocatalyst under visible irradiation, obtaining esterified oil with a 4.5% FFA content. The obtained product (esterified oil) is composed of a mixture of ethyl esters formed from the free fatty acids and also from the triglycerides. The results presented here demonstrate that $BiVO_4$ can be an efficient photocatalyst for the esterification of FFA present in WCO under visible irradiation, turning it into a great material for improving biodiesel production using more sustainable conditions.

Supplementary Information The online version contains supplementary material available at https://doi.org/10.1007/s11144-025-02808-0.

Acknowledgements The authors thank the: FINEP (01.220381.00), CNPq (313770/2020-4, 408661/2021-6 and 406026/2023-8), FAPEMIG (grants number BPD-00856-22; APQ-00889-18, APQ-03088-21, APQ-00282-21 and APQ-00370-22); FAPESP (Grant 2018/01258-5); CAPES (Finance Code 001 and 18/2020); MCTI/FINEP/FNDCT AÇÃO TRANSVERSAL ("SOS EQUIPAMENTOS 2021 AV 02"); SISNANO (CNPq proj #442575/2019-0); FAPEMIG (APQ-06609-24, APQ-00366-24); CNPq (406026/2023-8) and INCT Programs (CNPq proj #406925/2022-4).

Author contributions Camilo Aurélio B. Crisóstomo: Conceptualization; Methodology; Formal analysis; Investigation; Resources; Data curation; Writing—original draft; Writing—review & editing; Visualization. Fernanda Barbosa Damaceno: Conceptualization; Methodology; Investigation; Data curation; Writing—review & editing; João Paulo Mesquita: Investigation; Writing—review & editing; Funding acquisition. Juliana Arriel Torres: Investigation; Writing—review & editing; Caue Ribeiro: Investigation; Writing—review & editing; Roberto Ananias Ribeiro: Investigation; Writing—review & editing; Osmando F. Lopes: Investigation; Writing—review & editing; Waldir Avansi Jr: Investigation. Writing—review & editing; Jânio Santos Almeida: Investigation; Henrique A. J. L. Mourão: Conceptualization; Methodology; Investigation; Resources; Writing—review & editing; Supervision; Project administration; Funding acquisition.

Funding Funding was provided by Fundação de Amparo à Pesquisa do Estado de Minas Gerais (Grant Nos: APQ-00889-18, APQ-03088-21, APQ-00282-21 and APQ-00856-22; APQ-00370-22), Coordenação de Aperfeiçoamento de Pessoal de Nível Superior (Grant Nos: Code 001, 18/2020), Conselho Nacional de Desenvolvimento Científico e Tecnológico (Grant Nos: 313770/2020-4, 408661/2021-6, 406026/2023-8), and Fundação de Amparo à Pesquisa do Estado de São Paulo (Grant No: 2018/01258-5).

Data availability The full dataset supporting the findings of this study is available upon request to the corresponding author.

References

1. Wang Y, Torres JA, Shviro M, Carmo M, He T, Ribeiro C (2022) Photocatalytic materials applications for sustainable agriculture. Prog Mater 130(2022):100965. https://doi.org/10.1016/j.pmatsci.2022.100965
2. Cai, Kisch H (2008) Visible light induced photoelectrochemical properties of n-BiVO$_4$ and n-BiVO$_4$/p-Co$_3$O$_4$. J Phys Chem C 112(2):548–554. https://doi.org/10.1021/jp075605x
3. Afonso R, Serafim JA, Lucilha AC, Silva MR, Lepre LF, Ando RA, Dall'Antonia LH (2014) Photoelectroactivity of bismuth vanadate prepared by combustion synthesis: effect of different fuels and surfactants. J Braz Chem Soc 25:726–733. https://doi.org/10.5935/0103-5053.20140026
4. Hu Y, Fan J, Pu C, Li H, Liu E, Hu X (2017) Facile synthesis of double cone-shaped Ag$_4$V$_2$O$_7$/BiVO$_4$ nanocomposites with enhanced visible light photocatalytic activity for environmental purification. J Photochem Photobiol A 337:172–183. https://doi.org/10.1016/j.jphotochem.2016.12.035
5. Lopes OF, Carvalho KT, Macedo GK, de Mendonça VR, Avansi W, Ribeiro C (2015) Synthesis of BiVO$_4$ via oxidant peroxo-method: insights into the photocatalytic performance and degradation mechanism of pollutants. New J Chem 39(8):6231–6237. https://doi.org/10.1039/C5NJ00984G
6. Lopes OF, Carvalho KT, Nogueira AE, Avansi W Jr, Ribeiro C (2016) Controlled synthesis of BiVO$_4$ photocatalysts: evidence of the role of heterojunctions in their catalytic performance driven by visible-light. Appl Catal B 188:87–97. https://doi.org/10.1016/j.apcatb.2016.01.065
7. Malathi A, Madhavan J, Ashokkumar M, Arunachalam P (2018) A review on BiVO$_4$ photocatalyst: activity enhancement methods for solar photocatalytic applications. Appl Catal A 555:47–74. https://doi.org/10.1016/j.apcata.2018.02.010
8. Pelissari MR, Scalvi LVA, Dall'Antonia LH (2021) The role of PEG 6000 and PVP as stabilizing and surfactant agents in the photoelectrochemical properties of BiVO$_4$ monoclinic structure. J Braz Chem Soc 32(2021):1851–1864. https://doi.org/10.21577/0103-5053.20210076

9. Gonçalves HB, Freitas DV, Souza EJ, Melo MA, Gonzalez-Moya JR, Padrón-Hernández E, Machado G (2022) Photocatalytic performance of Ta_2O_5/$BiVO_4$ heterojunction for hydrogen production and methylene blue photodegradation. J Braz Chem Soc 33:894–905. https://doi.org/10.21577/0103-5053.20220002
10. Kim CW, Ji S, Kang MJ, Park H, Li F, Cheng HM, Kang YS (2019) Energy band edge alignment of anisotropic $BiVO_4$ to drive photoelectrochemical hydrogen evolution. Mat Today Energy 13:205–213. https://doi.org/10.1016/j.mtener.2019.05.011
11. Tayebi M, Lee BK (2019) Recent advances in $BiVO_4$ semiconductor materials for hydrogen production using photoelectrochemical water splitting. Renew Sustain Energy Rev 111:332–343. https://doi.org/10.1016/j.rser.2019.05.030
12. Kudo A, Hijii S (1999) H_2 or O_2 evolution from aqueous solutions on layered oxide photocatalysts consisting of Bi^{3+} with 6s2 configuration and d0 transition metal ions. Chem Lett 28(10):1103–1104. https://doi.org/10.1246/cl.1999.1103
13. Ribeiro CS, Brandestini MD, Moro CC, Lansarin MA (2019) A fair comparison between bismuth catalysts for application in photodegradation under visible and solar light. Braz J Chem Eng 36:201–208. https://doi.org/10.1590/0104-6632.20190361s20170498
14. Walsh A, Yan Y, Huda MN, Al-Jassim MM, Wei SH (2009) Band edge electronic structure of $BiVO_4$: elucidating the role of the Bi s and V d orbitals. Chem Mater 21(3):547–551. https://doi.org/10.1021/cm802894z
15. Zhao G, Liu W, Li J, Liang L (2016) Facile synthesis of hierarchically structured $BiVO_4$ oriented along (010) facets with different morphologies and their photocatalytic properties. Appl Surf Sci 390:531–539. https://doi.org/10.1016/j.apsusc.2016.08.126
16. Venkatesan R, Velumani S, Ordon K, Makowska-Janusik M, Corbel G, Kassiba A (2018) Nanostructured bismuth vanadate ($BiVO_4$) thin films for efficient visible light photocatalysis. Mater Chem Phys 205:325–333. https://doi.org/10.1016/j.matchemphys.2017.11.004
17. Ager JW, Shaner MR, Walczak KA, Sharp ID, Ardo S (2015) Experimental demonstrations of spontaneous, solar-driven photoelectrochemical water splitting. Energy Environ Sci 8(10):2811–2824. https://doi.org/10.1039/C5EE00457H
18. dos Santos WS, Almeida LD, Afonso AS, Rodriguez M, Mesquita JP, Monteiro DS, Pereira MC (2016) Photoelectrochemical water oxidation over fibrous and sponge-like $BiVO_{4/}\beta\text{-}Bi_4V_2O_{11}$ photoanodes fabricated by spray pyrolysis. Appl Catal B 182:247–256. https://doi.org/10.1016/j.apcatb.2015.09.034
19. da Silva MR, Dall'Antonia LH, Scalvi LVDA, dos Santos DI, Ruggiero LDO, Urbano A (2012) Deposition and characterization of $BiVO_4$ thin films and evaluation as photoanodes for methylene blue degradation. J Solid State Electrochem 16:3267–3274. https://doi.org/10.1007/s10008-012-1765-9
20. He Y, Zhang C, Hu J, Leung MK (2019) NiFe layered double hydroxide/$BiVO_4$ photoanode based dual-photoelectrode photocatalytic fuel cell for enhancing degradation of azo dye and electricity generation. Energy Procedia 158:2188–2195. https://doi.org/10.1016/j.egypro.2019.01.619
21. Kumar A, Sharma G, Naushad M, Kumar A, Kalia S, Mola GT (2017) Facile hetero-assembly of superparamagnetic Fe_3O_4/$BiVO_4$ stacked on biochar for solar photo-degradation of methyl paraben and pesticide removal from soil. J Photochem Photobiol A 337:118–131. https://doi.org/10.1016/j.jphotochem.2017.01.010
22. Hernández-Uresti DB, Alanis-Moreno C, Sanchez-Martinez D (2019) Novel and stable Fe-$BiVO_4$ nanocatalyst by efficient dual process in the ciprofloxacin degradation. Mater Sci Semicond Process 102:104585. https://doi.org/10.1016/j.mssp.2019.104585
23. Cheng L, Jiang T, Yan K, Gong J, Zhang J (2019) A dual-cathode photoelectrocatalysis-electroenzymatic catalysis system by coupling $BiVO_4$ photoanode with hemin/Cu and carbon cloth cathodes for degradation of tetracycline. Electrochim Acta 298:561–569. https://doi.org/10.1016/j.electacta.2018.12.086
24. Jiang H, Dai H, Deng J, Liu Y, Zhang L, Ji K (2013) Porous F-doped $BiVO_4$: synthesis and enhanced photocatalytic performance for the degradation of phenol under visible-light illumination. Solid State Sci 17:21–27. https://doi.org/10.1016/j.solidstatesciences.2012.12.009
25. Wang M, Xi X, Gong C, Zhang XL, Fan G (2016) Open porous $BiVO_4$ nanomaterials: electronspinning fabrication and enhanced visible light photocatalytic activity. Mater Res Bull 74:258–264. https://doi.org/10.1016/j.materresbull.2015.10.051
26. Corro G, Pal U, Tellez N (2013) Biodiesel production from Jatropha curcas crude oil using ZnO/SiO_2 photocatalyst for free fatty acids esterification. Appl Catal B 129:39–47. https://doi.org/10.1016/j.apcatb.2012.09.004

27. Corro G, Sánchez N, Pal U, Bañuelos F (2016) Biodiesel production from waste frying oil using waste animal bone and solar heat. Waste Manage 47:105–113. https://doi.org/10.1016/j.wasman.2015.02.001
28. Manique MC, Silva AP, Alves AK, Bergmann CP (2016) Application of hydrothermally produced TiO_2 nanotubes in photocatalytic esterification of oleic acid. Mater Sci Eng B 206:17–21. https://doi.org/10.1016/j.mseb.2016.01.001
29. Guo M, Jiang W, Chen C, Qu S, Lu J, Yi W, Ding J (2021) Process optimization of biodiesel production from waste cooking oil by esterification of free fatty acids using $La^{3+/}ZnO\text{-}TiO_2$ photocatalyst. Energy Convers Manage 229:113745. https://doi.org/10.1016/j.enconman.2020.113745
30. Khan M, Farah H, Iqbal N, Noor T, Amjad MZB, Bukhari SSE (2021) A TiO_2 composite with graphitic carbon nitride as a photocatalyst for biodiesel production from waste cooking oil. RSC Adv 11(59):37575–37583. https://doi.org/10.1039/D1RA07796A
31. Li Y, He R, Han P, Hou B, Peng S, Ouyang C (2020) A new concept: volume photocatalysis for efficient H_2 generation using low polymeric carbon nitride as an example. Appl Catal B 279:119379. https://doi.org/10.1016/j.apcatb.2020.119379
32. Li Y, Ji M, Ma Z, Meng L, Peng S (2022) Hierarchically porous polymeric carbon nitride as a volume photocatalyst for efficient H_2 generation under strong irradiation. Solar Rrl 6(2):2100823
33. Gao Y, Chen Y, Gu J, Xin Z, Sun S (2019) Butyl-biodiesel production from waste cooking oil: kinetics, fuel properties and emission performance. Fuel 236:1489–1495. https://doi.org/10.1016/j.fuel.2018.09.015
34. Aghel B, Mohadesi M, Ansari A, Maleki M (2019) Pilot-scale production of biodiesel from waste cooking oil using kettle limescale as a heterogeneous catalyst. Renew Energy 142(2019):207–214. https://doi.org/10.1016/j.renene.2019.04.100
35. Olivo A, Zanardo D, Ghedini E, Menegazzo F, Signoretto M (2018) Solar fuels by heterogeneous photocatalysis: from understanding chemical bases to process development. Chem Eng 2(3):42. https://doi.org/10.3390/chemengineering2030042
36. Dong F, Wu Q, Ma J, Chen Y (2009) Mild oxide-hydrothermal synthesis of different aspect ratios of monoclinic $BiVO_4$ nanorods tuned by temperature. Physica Status Solidi (a) 206(1):59–63. https://doi.org/10.1002/pssa.200723519
37. Avansi W, de Mendonça VR, Lopes OF, Ribeiro C (2015) Vanadium pentoxide 1-D nanostructures applied to dye removal from aqueous systems by coupling adsorption and visible-light photodegradation. RSC Adv 5(16):12000–12006. https://doi.org/10.1039/C4RA12788A
38. Murphy AB (2007) Band-gap determination from diffuse reflectance measurements of semiconductor films, and application to photoelectrochemical water-splitting. Sol Energy Mater Sol Cells 91(14):1326–1337. https://doi.org/10.1016/j.solmat.2007.05.005
39. Wetchakun N, Chaiwichain S, Inceesungvorn B, Pingmuang K, Phanichphant S, Minett AI, Chen J (2012) $BiVO_4/CeO_2$ nanocomposites with high visible-light-induced photocatalytic activity. ACS Appl Mater Interfaces 4(7):3718–3723. https://doi.org/10.1021/am300812n
40. Tokunaga S, Kato H, Kudo A (2001) Selective preparation of monoclinic and tetragonal $BiVO_4$ with scheelite structure and their photocatalytic properties. Chem Mater 13(12):4624–4628. https://doi.org/10.1021/cm0103390
41. Mohamed HEA, Afridi S, Khalil AT, Zohra T, Alam MM, Ikram A, Maaza M (2019) Phytosynthesis of $BiVO_4$ nanorods using Hyphaene thebaica for diverse biomedical applications. AMB Express 9:1–14. https://doi.org/10.1186/s13568-019-0923-1
42. Lopes OF, Carvalho KT, Avansi W, Milori DM, Ribeiro C (2018) Insights into the photocatalytic performance of $Bi_2O_2CO_3/BiVO_4$ heterostructures prepared by one-step hydrothermal method. RSC Adv 8(20):10889–10897. https://doi.org/10.1039/C8RA00605A
43. Zhang A, Zhang J (2009) Characterization of visible-light-driven $BiVO_4$ photocatalysts synthesized via a surfactant-assisted hydrothermal method. Spectrochim Acta Part A Mol Biomol Spectrosc 73(2):336–341. https://doi.org/10.1016/j.saa.2009.02.028
44. Serafim JA, Afonso R, Lucilha AC, Oliveira LAD, Silva PRCD, Silva MRD, Dall'Antonia LH (2014) Vanadato de bismuto sintetizado por combustão em solução na presença de diferentes combustíveis: síntese, caracterização e estudo da atividade fotocatalítica. Quim Nova 37(2014):1158–1164. https://doi.org/10.5935/0100-4042.20140191
45. Šurca A, Orel B (1999) IR spectroscopy of crystalline V_2O_5 films in different stages of lithiation. Electrochim Acta 44(18):3051–3057. https://doi.org/10.1016/S0013-4686(99)00019-5
46. Park HS, Leonard KC, Bard AJ (2013) Surface interrogation scanning electrochemical microscopy (SI-SECM) of photoelectrochemistry at a W/Mo-$BiVO_4$ semiconductor electrode: quantification of

hydroxyl radicals during water oxidation. J Phys Chem C 117(23):12093–12102. https://doi.org/10.1021/jp400478z

47. Jang YJ, Simer C, Ohm T (2006) Comparison of zinc oxide nanoparticles and its nano-crystalline particles on the photocatalytic degradation of methylene blue. Mater Res Bull 41(1):67–77. https://doi.org/10.1016/j.materresbull.2005.07.038
48. Liu L, Li H, Zhang Y (2006) A comparative study on catalytic performances of chromium incorporated and supported mesoporous MSU-x catalysts for the oxidehydrogenation of ethane to ethylene with carbon dioxide. Catal Today 115(1–4):235–241. https://doi.org/10.1016/j.cattod.2006.02.040

Authors and Affiliations

Camilo Aurélio Brandão Crisóstomo[1] · Fernanda Barbosa Damaceno[1] · João Paulo de Mesquita[1] · Juliana Arriel Torres[2] · Caue Ribeiro[2] · Roberto Ananias Ribeiro[3] · Osmando F. Lopes[4] · Waldir Avansi Jr.[5] · Jânio Santos Almeida[1] · Henrique Aparecido de Jesus Loures Mourão[1,6]

✉ Camilo Aurélio Brandão Crisóstomo
camiloaurelioeq@gmail.com

[1] Chemistry Postgraduate Program (PPGQ), Federal University of Jequitinhonha and Mucuri Valleys (UFVJM), MGT 367 Highway, Km 583, Diamantina, MG CEP 39100-000, Brazil

[2] Embrapa Instrumentation São Carlos, XV de Novembro, 1452, Centro, São Paulo, SP CEP 13560-970, Brazil

[3] Federal Institute of Northern Minas Gerais (IFNMG), MG 404 Highway, Km 02, Salinas, MG CEP 39560-000, Brazil

[4] Laboratory of Photochemistry and Materials Science, Institute of Chemistry, Federal University of Uberlândia (UFU), João Naves de Ávila, Uberlândia, MG CEP 38400-902, Brazil

[5] Department of Physics, Federal University of São Carlos (UFSCar), Washington Luís, Monjolinho, São Carlos, SP CEP 13565-905, Brazil

[6] Institute of Science and Technology, Federal University of the Jequitinhonha and Mucuri Valleys (UFVJM), Rodovia MGT 367, Km 583, Diamantina, MG CEP 39100-000, Brazil